Analyst

ROYAL SOCIETY OF CHEMISTRY

PAPER

View Article Online
View Journal | View Issue

Cite this: *Analyst*, 2024, **149**, 5277

Surface-enhanced Raman scattering enhancement using a hybrid gold nanoparticles@carbon nanodot substrate for herbicide detection†

Naghmeh Aboualigaledari,[a] Anitha Jayapalan,[a] Panesun Tukur,[a] Mengxin Liu,[a] Frank Tukur,[a] Yanling Zhang,[c] Gerald Ducatte,[c] Madan Verma,[c] Janet Tarus,[c] Simona E. Hunyadi Murph *[b] and Jianjun Wei *[a]

The widespread distribution of herbicides in the environment poses a significant risk to human health and wildlife. Surface-enhanced Raman scattering (SERS) has emerged as a powerful technique for detecting and analyzing herbicides. However, developing a low-cost, highly sensitive, reproducible, stable, and Raman-active nanostructured substrate for herbicide detection remains a particular challenge. In this research, a nanohybrid substrate consisting of gold nanoparticles@carbon nanodots (AuNPs@CNDs) was synthesized by reducing $HAuCl_4$ in the presence of CNDs at 100 °C. The optical, chemical, and physical properties of CNDs, AuNPs, and the hybrid AuNPs@CND substrates were thoroughly investigated using various techniques including UV-vis spectrometry, Raman spectroscopy, X-ray photoelectron spectroscopy (XPS), scanning electron microscopy (SEM), transmission electron microscopy (TEM), and CytoViva darkfield and hyperspectral imaging. The SERS effect of the substrates was evaluated using rhodamine 6G (Rh6G), a Raman-active probe, and two groups of herbicides containing mesotrione or S-metolachlor. The results demonstrated a significant signal amplification in the SERS spectra of Rh6G and herbicide molecule detection using the AuNPs@CND substrate compared to bare CNDs and AuNPs alone. This suggests that the nanohybrid AuNPs@CND SERS substrate holds promise for the detection of herbicides and other organic compounds in environmental applications.

Received 7th May 2024,
Accepted 28th August 2024

DOI: 10.1039/d4an00649f

rsc.li/analyst

1. Introduction

The widespread distribution of herbicides in the environment poses a significant risk to human health and wildlife.[1] Accurate, quantitative monitoring of herbicide residues, especially in water environments, is critical for their management, removal or treatment. Traditionally, a broad range of analytical methods, such as gas chromatography (GC),[2] high performance liquid chromatography (HPLC), GC-mass spectrometry (GC-MS), electrochemical and spectrophotometric techniques, have been used for the extraction and determination of their concentration.[3–6] Advancements in nanomaterials and nanotechnology have provided alternative advantageous sensor technologies, such as nano-electrochemical sensors,[7] molecularly imprinted polymers,[8] and nanoplasmonic surface enhanced Raman spectroscopy (SERS),[9] which may enable easy operation, improved sensitivity, portability and real-time and on-site applications.

The surface-enhanced Raman scattering (SERS) technique relies on plasmonic metallic nanostructures to concentrate electromagnetic energy, thereby enhancing the molecular Raman signal. SERS spectroscopy is a powerful technique with diverse applications in medical science and analytical chemistry.[10] Tailored nanostructures enable fast, sensitive, nondestructive, and highly efficient detection of probe molecules, even facilitating single molecule analysis.[11–13] In SERS, the amplification of the Raman signals of probe molecules results from the excitation of localized surface plasmon resonance (LSPR) at the metal–dielectric interface of the substrate. Therefore, the magnitude of SERS enhancement critically depends on the SERS substrate.[14]

Gold and silver nanostructures are typical metals used as SERS substrates due to their LSPR bands covering the visible and near-infrared (NIR) wavelength regimes necessary to excite

[a]*Department of Nanoscience, Joint School of Nanoscience and Nanoengineering, University of North Carolina at Greensboro, Greensboro, NC 27401, USA. E-mail: j_wei@uncg.edu*
[b]*Environmental and Legacy Management Department, Savannah River National Laboratory (SRNL), Aiken, SC, 29808, USA. E-mail: Simona.Murph@srnl.doe.gov*
[c]*Syngenta Crop Protection Inc., Greensboro, NC 27409, USA*

† Electronic supplementary information (ESI) available: UV-vis and SERS spectra for synthesis optimization, additional TEM, XPS spectra, SERS spectra, and calibration curves. See DOI: https://doi.org/10.1039/d4an00649f

Raman modes.[15–18] While silver nanoparticles (AgNPs) offer higher plasmon enhancement, they are susceptible to oxidation, leading to poor stability.[19] In contrast, gold exhibits superior chemical stability.[20,21] Recent SERS studies have focused on developing and optimizing substrates with promising enhancement effects.[22–25] For instance, a gold nanorod array was developed and optimized for SERS detection of the herbicide atrazine.[26] With advancements in nanotechnology, SERS substrates have evolved from single-composition nanomaterials to multi-component nanomaterials.[27] This is due to their ability to serve as multi-modal platforms for enhanced sensing of analytes, sorbent capability, and magnetic recyclability, among others.[28] Hybrid nanomaterials and complex nanostructures comprising carbon nanomaterials and metal NPs, such as AuNPs, have demonstrated exceptional SERS enhancement capabilities.[29,30]

Carbon dots (CDs) with diameters usually less than 10 nm are classified as carbon quantum dots (CQDs), carbon nanodots (CNDs), and graphene QDs (GQDs).[31] Compared to conventional semiconductor quantum dots and semiconductors, CNDs offer advantages such as low toxicity, excellent biocompatibility, multifunctionality, and straightforward synthesis.[32–34] CNDs represent a novel class of carbon nanomaterials characterized by a spherical morphology and typically an amorphous lattice structure. The functional groups present in CNDs play a crucial role in enhancing surface-enhanced Raman scattering (SERS). These functional groups are typically introduced during hydrothermal synthesis through doping heteroatoms like nitrogen (N), sulfur (S), boron (B), phosphorus (P), and others.[35–38]

Recent findings indicate that N-doped CNDs contribute to the improvement of SERS signals, likely because N-doped CNDs facilitate excited state charge transfer to the target molecule through π–π interactions.[39–41] By incorporating CNDs as a shell component into AuNPs with optimized thickness, the chemical enhancement can be improved. This enhancement occurs through increased adsorption of analytes and the prevention of signal interference from probe molecules caused by direct contact with gold surfaces.[42]

The utilization of AuNPs achieves high SERS enhancement due to their appropriate size, shape, and matching of the laser line with the AuNPs' LSPR, which leads to an increase in the surface area and local electromagnetic (EM) field enhancement.[42] Previous studies have demonstrated the effectiveness of AuNPs or silver NP-based SERS substrates for detecting herbicides, including atrazine, diquat, flumetsulam, glyphosate, paraquat, and prometryn.[26,43–52] SERS detection of relatively new types of herbicides, such as mesotrione and S-metolachlor, has been rarely reported. In this study, microwave-synthesized hybrid AuNP@CND core–shell composite NPs are optimized for Raman signal amplification as SERS probes for the sensitive detection of mesotrione and S-metolachlor molecules, which are notably the active components in the formulation complex. This approach capitalizes on the advantageous synergistic effects of both chemical and EM field enhancement from the CND and AuNP components,[29] thereby improving SERS sensing capabilities.

2. Materials and methods

2.1. Chemicals and reagents

Hydrogen tetrachloroaurate ($HAuCl_4$) solution (from Fisher Scientific, Au 44% w/w), sodium citrate (from Fisher Scientific, ≥99%), rhodamine 6G (from ACROS Organics, 99%), citric acid (from ACROS Organics, 99%), and ethylenediamine (EDA, from Fisher Scientific, 99%) were utilized in this study without further purification.

The herbicides used in the research, including mesotrione (2-(4-methylsulfonyl-2-nitrobenzoyl)cyclohexane-1,3-dione, ZA1296E), A12738A formulation, and S-metolachlor ((S)-2-chloro-*N*-(2-ethyl-6-methyl-phenyi)-*N*-(2-methoxy-1-methyl-ethyl)-acetamide, CGA77102), as well as its formulation LUMAX EZ (A19414A), were obtained from Syngenta Crop Protection, LLC.

2.2. Materials characterization

The morphology of both the AuNPs and AuNPs@CNDs was examined using field-emission scanning electron microscopy (FE-SEM) conducted with a Carl Zeiss Auriga-BU FIB FESEM Microscope. The measurements were performed at an accelerating voltage of 5.0 kV. Additionally, transmission electron microscopy (TEM) was employed using a Carl Zeiss Libra 120 PLUS instrument to further investigate the morphology.

The elemental composition of the samples was determined using X-ray photoelectron spectroscopy (XPS) utilizing a Thermo Scientific ESCALAB Xi+ instrument. Raman spectroscopy was conducted using a Horiba XploRA One Raman Confocal Microscope system, with a 532 nm laser serving as the excitation source.

To assess the optical properties of the CNDs, AuNPs, and AuNPs@CNDs, ultraviolet-visible spectrophotometry was performed using a Varian Cary 6000i spectrophotometer. Fluorescence spectrophotometry was carried out using a Varian Cary Eclipse instrument. A Varian Agilent 710 inductively coupled plasma optical emission spectrometer (ICP-OES) with trace elemental analysis capability for wavelengths from 177 to 785 nm was used to determine the concentration of Au in AuNPs@CND and AuNP suspensions.

2.3. Nanoparticle synthesis

2.3.1. Synthesis of CNDs. The synthesis of CNDs involved a microwave-assisted procedure conducted at 300 W for 18 minutes. A water solution containing ethylenediamine and citric acid as precursors was utilized by following a previously reported procedure.[32] Following the synthesis, the solution underwent purification using centrifugation for 20 minutes. Subsequently, it was dialyzed for 48 hours against deionized (DI) water. The resulting solution was then freeze-dried for 24 hours to obtain a solid sample.

2.3.2. Synthesis of AuNPs. Gold nanoparticles (AuNPs) were synthesized following the method introduced by Frens,[53,54] which relies on the citrate reduction of $HAuCl_4$. Initially, a 25 mL solution of $HAuCl_4$ (0.01% by weight) was heated to 97 °C. After 15 minutes of temperature stabilization, 375 μL of an aqueous solution of sodium citrate (1% by

weight) was swiftly added to the gold solution under continuous stirring, maintaining the temperature at 100 °C. Following a 30-minute reaction period, a wine-red suspension containing AuNPs was obtained. Subsequently, the suspension was cooled to room temperature over a 15-minute period while being magnetically stirred. The mixture underwent dialysis using a 1 kDa dialysis membrane for 24 hours to eliminate any unreacted precursor molecules.

2.3.3. Synthesis of AuNPs@CNDs. The hybrid AuNPs@CNDs were synthesized through the reduction of $HAuCl_4$ in the presence of CNDs at 100 °C, similar to a reported procedure.[53] In this method, a 150 μL aqueous solution of $HAuCl_4$ (1 mg mL^{-1}) was added to a 3 mL solution of CNDs (0.12 mg mL^{-1}). The mixed solution was maintained at 100 °C for 80 minutes. Subsequently, the mixture was allowed to cool to room temperature and then dialyzed using a 1 kDa dialysis membrane for 24 hours to eliminate any unreacted precursor molecules. By adjusting the feeding mass ratio of $HAuCl_4$ to CNDs, AuNPs@CNDs with different sizes can be obtained. At first, CND solutions with concentrations ranging from 0.09, 0.11, and 0.12 mg mL^{-1} were added to a 150 μL solution of $HAuCl_4$ (1 mg mL^{-1}) to achieve $HAuCl_4$/CNDs with mass ratios of 2.4, 2.2, and 1.8, respectively. It was observed that the minimum concentration of CNDs that resulted in the formation of AuNPs@CNDs was 0.12 mg mL^{-1}. Then, the concentration of CNDs was maintained constant at 0.12 mg mL^{-1} and different volumes of $HAuCl_4$ ranging from 70 to 190 μL (yielding $HAuCl_4$/CNDs with mass ratios of 5.2, 3.3, 2.4, and 1.9, respectively) were added to the CNDs to produce hybrid AuNPs@CNDs with different sizes for the following SERS studies.

2.3.4. SERS measurements of Rh6G and herbicides using NPs. For the SERS measurements of Rh6G, a 10 μL aliquot of Rh6G aqueous solution was mixed with 50 μL of AuNPs@CND, AuNP, and CND aqueous suspensions, respectively, and the mixed suspension was sonicated for 30 min. Thereafter, 60 μL of each sample was added dropwise on a cover glass substrate and the samples were air-dried for 3 hours in a fume hood. Note that the AuNP and AuNPs@CND solutions have the same particle concentration of 0.0585 mg mL^{-1} measured by ICP-OES, and the concentration of CNDs was 0.12 mg mL^{-1}. The SERS measurements were performed using a Horiba XploRA Raman Confocal Microscope using 532 nm light excitation, a 50× objective, an 1800 gr per nm grating, and an acquisition and accumulation time of 5 s.

To record the SERS spectra of 4 herbicide samples, 10 μL of each herbicide sample were added to 50 μL of AuNPs@CND aqueous suspension and sonicated for 30 min. The mixture of samples was dried on cover glasses for 3 h in a fume hood. SERS spectra were obtained on dried samples using 532 nm excitation, a 50× objective, a 1200 gr per nm grating, an accumulation time of 5 s, and an acquisition time of 35 s.

The first group of herbicides included CGA77102 (S-metolachlor, 86.6% by weight) and A19414A formulation (S-metolachlor, 27.1% by weight). The sample solutions containing the desired concentrations of CGA77102 and A19414A formulation ranging from 10^{-12}–10^{-3} M were analysed with respect to the effective S-metolachlor component without extraction. The same procedure was carried out for the second group of herbicides, ZA1296E (mesotrione, 60.0 by wt%) and A12738A formulation (mesotrione, 40.0 wt%).

3. Results and discussion

3.1. Characterization of CNDs, AuNPs, and AuNPs@CNDs

The size and morphology of the NPs were characterized using SEM and TEM. The SEM and TEM images of AuNPs (Fig. 1A) reveal the spherical shape of AuNPs with a size of approximately 50 nm, consistent with the 540 nm absorption of the

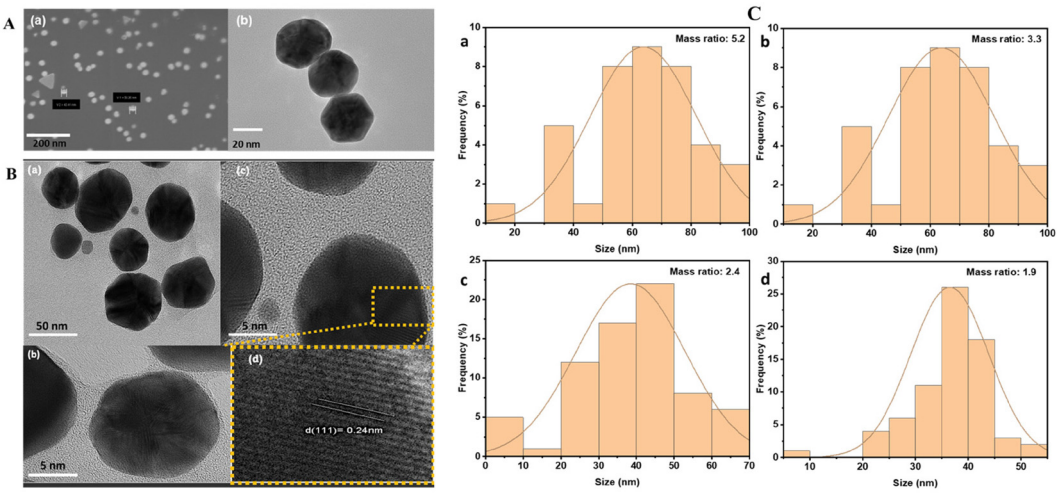

Fig. 1 (A). SEM image (a) and HR-TEM image (b) of the AuNPs; (B) TEM image (a), HR-TEM images (b and c) and zoomed-in view of the lattice fringe of the crystalline structure; and (C) the histogram of the size distribution of AuNPs@CNDs synthesized with different $HAuCl_4$/CND mass ratios of 5.2, 3.3, 2.4, and 1.9 from (a) to (d).

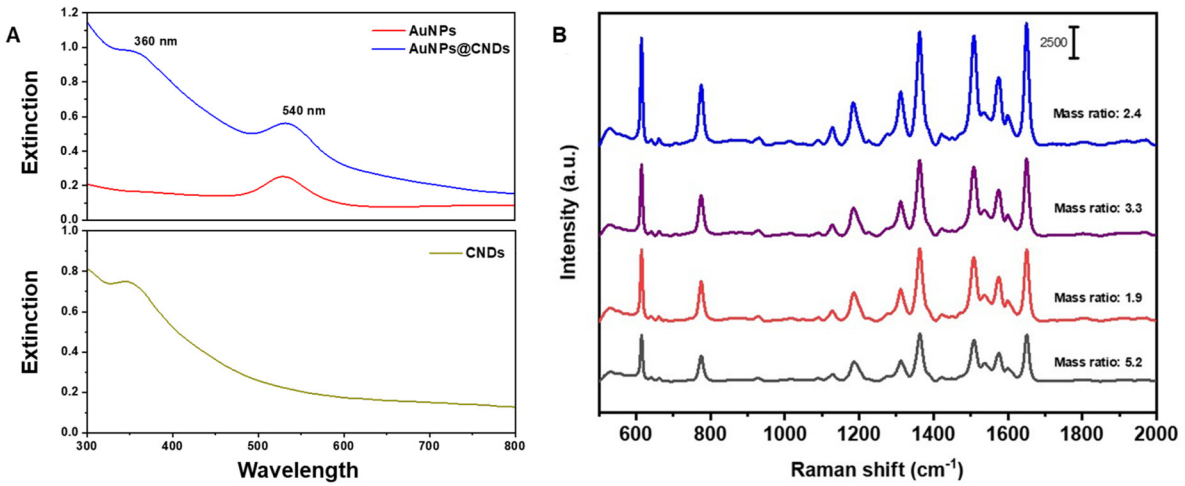

Fig. 2 (A) UV-Vis absorption spectra of AuNPs, CNDs and hybrid AuNPs@CNDs and (B) SERS spectra of Rh6G with the hybrid AuNPs@CNDs generated with different mass ratios.

UV-vis spectra of AuNPs (Fig. 2A). The TEM images of hybrid AuNPs@CNDs (Fig. S1A†) at different $HAuCl_4$/CND mass ratios (5.2, 3.3, 2.4, and 1.9) show that the AuNPs@CNDs obtained with the mass ratio of 2.4 have a spherical shape and the NPs are not agglomerated and more uniformly distributed compared to the other mass ratios. To confirm the hybrid structure of AuNPs@CNDs, SEM and energy dispersive X-ray spectroscopy (EDS) were applied to map the elemental distribution. Fig. S1B† shows the carbon-capped core–shell configuration. Additionally, the HR-TEM images of 2.4-ratio AuNPs@CNDs (Fig. 1B) suggest successful wrapping of AuNP cores by CND structures. Fig. 1B(d) confirms a 0.24 nm lattice fringe of its crystalline structure corresponding to the (111) planes of AuNPs.[55] The size distribution of AuNPs@CNDs as a function of the $HAuCl_4$/CND mass ratio is shown in Fig. 1C and AuNPs@CNDs with a mass ratio of 2.4 have a size range between 40 and 50 nm, similar to a previous report.[53] It is known that carboxylate and nitrogen-containing groups including amine and pyridine have a strong binding affinity to gold,[56,57] which allows the CNDs to act as a capping agent that wraps around the surface of AuNPs to form a core–shell structure.

To further confirm the formation of hybrid AuNPs@CNDs, UV-visible absorption spectra were recorded and compared with those of three samples, *i.e.*, the AuNPs, CNDs and the hybrid. In Fig. 2A, the spectrum of AuNPs shows a SPR peak at 540 nm, which indicates the formation of AuNPs with a size of around 50 ± 7 nm.[42] The absorption spectrum of CNDs displays a typical peak at 360 nm, which is attributed to the n–π* transition of C═O.[58] The absorption spectrum of AuNPs@CNDs presents both the plasmon absorption peak at 540 nm of the AuNP core[53] and the 360 nm peak for CNDs, corroborating the production of the hybrid NPs. Comparing the UV-vis absorption from different mass ratio products (Fig. S2†), the 2.4 mass ratio AuNPs@CNDs have the highest plasmonic peak around 540 nm along with a distinct peak at 360 nm for the CNDs, implying potential for Raman signal enhancement.

The SERS performance of the hybrid AuNPs@CND substrates obtained from different mass ratios was evaluated using Rh6G. Fig. 2B presents the SERS spectra of Rh6G at a concentration of 48×10^{-8} M using AuNPs@CND substrates produced from different $HAuCl_4$/CND mass ratios. It is apparent that the 2.4 ratio hybrid substrate provides the best SERS signal enhancement of Rh6G, plausibly due to the size range of the generated AuNPs and optimum surface coverage. The results further confirm the plasmonic properties observed in the UV-vis spectra. Therefore, the 2.4 mass ratio AuNPs@CND hybrid substrate is selected for further investigation and applied in herbicide sensing studies.

The structural, composition and spectroscopic properties of the synthesized NPs were further performed and analyzed. The Raman spectra of both CNDs and AuNPs@CNDs (Fig. S3a†) show two distinct peaks at 1340 cm^{-1} and 1590 cm^{-1}, which correspond to the D and G bands of the carbon component, respectively. The D band corresponds to structural defects in graphitic sp^3-hybridized carbon, whereas the G band is related to the vibration of sp^2 carbon atoms in a 2D hexagonal lattice.[59,60] The relative intensity of D and G bands (D/G ratio) in the Raman spectra of AuNPs@CNDs is 0.780, whereas this ratio is 0.741 for CNDs. The D and G band intensities of AuNPs@CNDs are much higher than those of CNDs, suggesting the enhanced defect effect of AuNPs.[61,62] The photoluminescence (PL) spectra of CNDs and AuNPs@CNDs (Fig. S3b†) show that the PL intensity of AuNPs@CNDs is decreased compared to that of CNDs when excited with 360 nm light, which indicates that the PL of CNDs is quenched in the AuNPs@CND system. This phenomenon is attributed to a photo-induced electron transfer process between the CNDs and AuNPS.[53,61]

The full XPS scan spectra of CNDs and AuNPs@CNDs exhibit three peaks at 285.5, 399.0 and 531.0 eV, which are attributed to C 1s, N 1s, and O 1s, respectively.[63] Compared to

the XPS spectrum of CNDs, the XPS spectrum of AuNPs@CNDs presents a peak of the Au element at 335 eV (Fig. S4a and b†). The C 1s XPS spectra of CNDs and AuNPs@CNDs (Fig. S4d and e†) show peaks at 284.3, 285.4, and 287.5 eV, which are attributed to C–C, C–O–C, and O–C═O groups, respectively. The N 1s XPS spectra shown in Fig. S4c† feature two peaks corresponding to pyridinic nitrogen (398 eV) and pyridone nitrogen (399.6 eV).[64] The O 1s band (Fig. S4f†) can be deconvoluted into two peaks located at 531.4 and 531.9 eV, which represent the C–O and C═O groups, respectively.

A dark-field CytoViva hyperspectral imaging system was used to measure light scattering from AuNPs and AuNPs@CNDs distributed on a glass substrate. A CytoViva hyperspectral imaging system enables both optical and hyperspectral imaging of samples, which can be used for spectral characterization and spectral mapping of nanoscale samples.[58,65] In experimental measurement, unpolarized plain light (broad band) from a halogen lamp was used as incident light to illuminate the nanoparticle samples from the top. The reflecting light signal captured by a 60× objective lens is then collected using a darkfield CytoViva hyperspectral imaging system (Fig. 3). The peak at around 550 nm corresponds to the SPR of AuNPs, which is in accordance with the UV-vis spectra and confirms that the SPR of AuNPs occurs at around 540 nm. It is noteworthy that the peak at around 580 nm can be attributed to the SPR of the aggregation of AuNPs.[66] The intensities of the SPR peaks of AuNPs@CNDs are much higher than those of AuNPs, suggesting the enhancement effect of AuNPs@CNDs. A new resonant mode located at 615 nm appeared after AuNPs are covered by CNDs, and this is probably because of coupling between AuNPs and CNDs.[55]

3.2. SERS properties of NPs

Rh6G was used as a Raman reporter to perform the SERS evaluation using three NPs, *i.e.*, AuNPs@CNDs, CNDs, and AuNPs, prior to the application in herbicide detection. Fig. 4A displays the SERS spectra of 48 × 10^{-8} M Rh6G after mixing with AuNPs@CNDs, AuNPs, CNDs, respectively, and Rh6G only for comparison. An obviously increased SERS signal was observed from the AuNPs@CND hybrid substrate. The great signal amplification (>10×) of the main signature peaks of Rh6G obtained using AuNPs@CNDs was obtained compared to that obtained using the AuNPs for Rh6G. The band at 614 cm^{-1} was assigned to the C–C–C ring in-plane in the xanthene ring, whereas those around 771, 1127, and 1183 cm^{-1} were attributed to the C–H ring in the xanthene or phenyl ring.[67] The prominent peaks in the range of 1311, 1362, 1507, 1573, and 1650 cm^{-1} were due to the symmetric modes of in-plane C–C stretching vibrations in the xanthene or phenyl ring, which are the characteristic Raman scattering features of Rh6G.[20,68] These results confirm that the hybrid AuNPs@CND system can significantly improve the SERS performance in terms of signal enhancement, implying enhanced sensitivity and accuracy for sensing applications.

Next, we collected the SERS responses of Rh6G at different concentrations ranging from 48 × 10^{-12} to 48 × 10^{-8} M using the same AuNPs@CND substrate. Fig. 4B shows that there is an increase in the Raman signal intensity of the characteristic Rh6G peaks upon increasing the concentration of Rh6G. By plotting $\log I_{1650}$ (logarithm of SERS peak intensity at 1650 cm^{-1}) *versus*

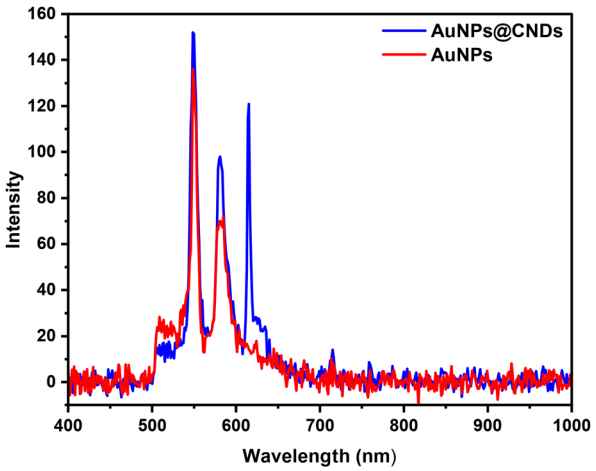

Fig. 3 The extracted reflection spectra obtained from the CytoViva hyperspectral imaging measurements.

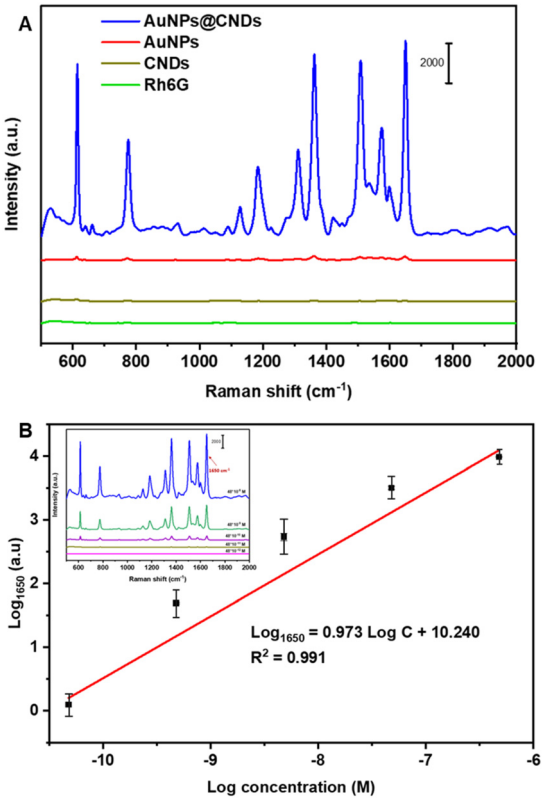

Fig. 4 (A) SERS spectra of Rh6G (48 × 10^{-8} M) using CNDs, AuNPs, and AuNPs@CNDs, respectively. (B) Raman signal at 1650 cm^{-1} *vs.* Rh6G concentration on a logarithmic scale using AuNPs@CNDs for SERS measurement; the inset shows the SERS spectra at different concentrations of Rh6G.

log C (logarithm of Rh6G concentration), a linear calibration curve was obtained, where the square coefficient of determination (R^2) is 0.991, demonstrating a linear relationship between the Raman intensity and the concentration.

The reproducibility and stability of the SERS substrate for sensing are important for the detection of analytes of interest, especially when deployed in the field.[9] The SERS responses collected at 18 random points on the same sample using AuNPs@CNDs and 48×10^{-8} M Rh6G display the uniformity of the sample (Fig. 5A) based on a standard deviation of 0.9% from the peak intensity at 1650 cm^{-1}. The uniformity in SERS signals recorded confirms the good reproducibility and homogeneity of using the hybrid AuNPs@CNDs in sample preparation and detection. Furthermore, to confirm the batch-to-batch reproducibility, 6 different batches of AuNPs@CND substrates were used for SERS measurement of Rh6G and the SERS intensity at the 1650 cm^{-1} peak was recorded at 3 random points of each substrate. Fig. 5B demonstrates the averaged Raman intensity for the six samples, showing excellent reproducibility. The UV-visible spectra of AuNPs@CNDs and SERS spectra of 48×10^{-8} M Rh6G with AuNPs@CNDs in Fig. 5C and D show their stability during storage for up to 60 days, respectively. There are no significant changes in both spectra, which confirms the high stability of the hybrid AuNPs@CND substrate.

3.3. SERS detection of herbicide molecules

The 2.4-ratio AuNPs@CND substrate in solution was further applied for the detection of two different groups of herbicides. As described in the Experimental section, the first group of herbicides includes CGA77102 (S-metolachlor, 86.6 wt%) and A19414A formulation (S-metolachlor, 27.1 wt%). S-metolachlor is a member of the chloroacetanilide family of herbicides, which is used for grass and broadleaf controls in corn, soybean, *etc*. The signal amplification of the main Raman peaks at 994.4 and 989.6 cm^{-1} obtained using AuNPs@CNDs compared to that of bare AuNPs is calculated to be 10.8 and 7.3-fold for CGA77102 and A19414A, respectively (Fig. S5a and b†).

The second group of herbicides includes ZA1296E (mesotrione, 60 wt%) and A12738A formulation (mesotrione, 40 wt%) with the main effective component of mesotrione. Mesotrione has an aromatic ketone and is a toxic synthetic herbicide in the agriculture industry for the selective contact and residual control of broadleaf weeds in field corn. According to Fig. S5c and d,† the SERS peaks at 1526, 1552, and 1608 cm^{-1} are attributed to the C=C stretching in carotenoids, the central 16-membered-ring vibrations and the C–C stretching of the pyrrole ring in chlorophyll, and the ν phenyl ring in phenolic compounds, respectively.[69] Similarly, the hybrid AuNPs@CNDs provide greater Raman signal enhancement than the AuNPs.

Fig. 6 shows the SERS spectra of the four herbicide samples using the hybrid AuNPs@CNDs as Raman enhancement probes. The spectra of CGA77102 and A19414A with different concentrations indicate a decline in Raman signal intensity along with decreasing concentration. Similarly, the SERS spectra of ZA1296E and A12738A at different concentrations show a decline in Raman intensity with decreasing concentration. Linear calibration curves as a function of the herbicide

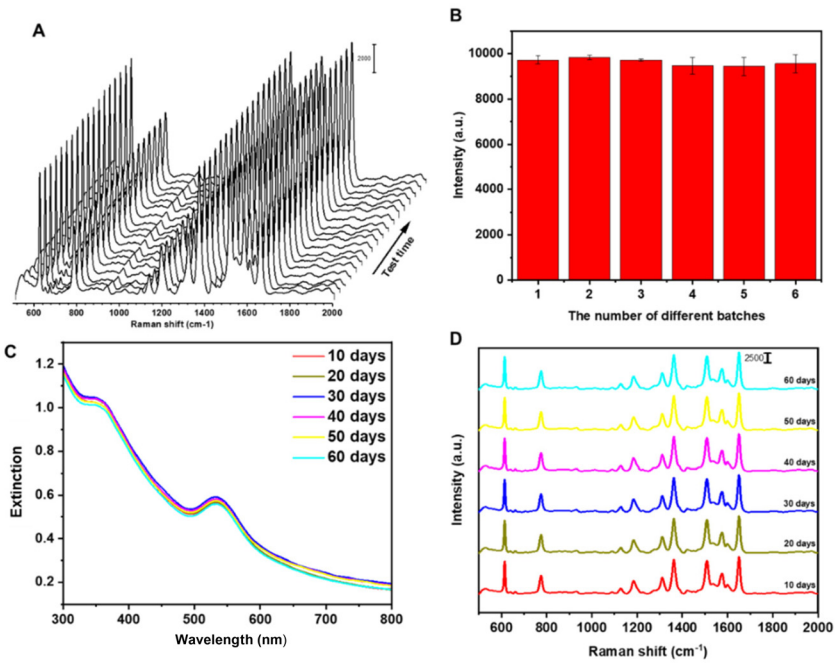

Fig. 5 (A) Multiple point Raman signal collection profiles of AuNPs@CNDs with an Rh6G concentration of 48×10^{-8} M; (B) Raman signal intensity at 1650 cm^{-1} of Rh6G with 6 different batches of AuNPs@CNDs; (C) UV-vis spectra of AuNPs@CNDs stored for a period of 10–60 days; and (D) SERS spectra of 48×10^{-8} M Rh6G with AuNPs@CNDs for a period of 10–60 days.

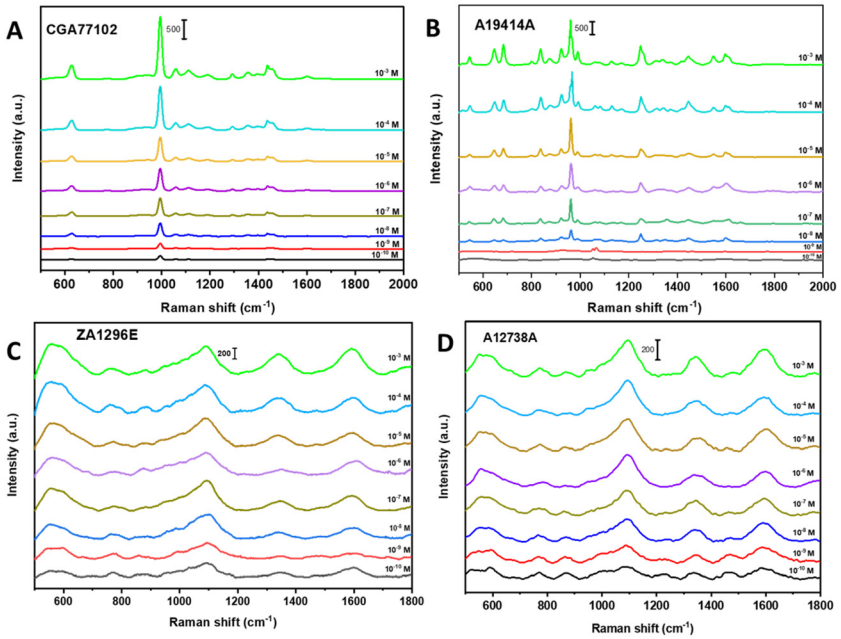

Fig. 6 SERS spectra of (A) CGA77102 and (B) A19414A formulation at different concentrations, and (C) ZA1296E and (D) A12738A formulation at effective component concentrations ranging from 10^{-3} to 10^{-10} M using AuNPs@CNDs.

concentration ranging from 10^{-10} to 10^{-3} M are achieved by plotting $\log I_{994.4}$ and $\log I_{989.6}$ *versus* $\log C$ for CGA77102 and A19414A (Fig. 7A and B), which demonstrate a linear detection response with R^2 values of 0.984 and 0.970, respectively. The lowest detection limit (LOD) is estimated to be 0.1 nM using a signal/noise ratio of 3.[32] A small shift of the characteristic

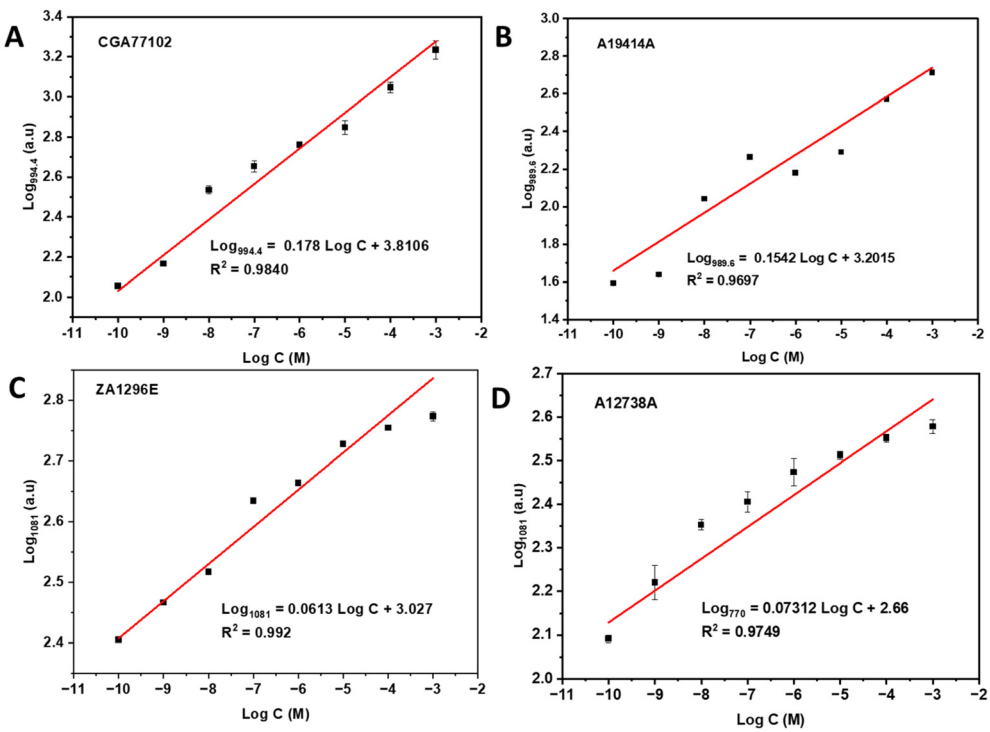

Fig. 7 Calibration curves plotted with the logarithm of Raman signal intensity *vs.* concentration using the marker peak intensity for CGA77102 at 994.4 cm^{-1} (A) and A19414A at 989.6 cm^{-1} (B), ZA1296E at 1081 cm^{-1} (C), and A12738A at 770 cm^{-1} (D). Each data point in this figure is the mean value of triplicate measurements.

peak position between CGA77102 and A19414A (994.4 *vs.* 989.6 cm^{-1}) could be attributed to the different components in the original samples or interaction between the substrates and analytes. The logarithm of the SERS intensity of the 1081 cm^{-1} peak *versus* the logarithm of the concentration of ZA1296E and A12738A in the range of 10^{-10}–10^{-3} M was plotted with good linearity with R^2 = 0.992 and 0.9749, respectively, as shown in Fig. 7C and D.

3.4 Detection of herbicides in tap water and recovery experiments

To test the capability of using the hybrid AuNPs@CNDs as a Raman probe for herbicide detection, we spiked tap water with herbicide samples and obtained the SERS spectra to evaluate the recovery rate, *i.e.*, the percentage of the measured concentration relative to the spiked concentration. In these experiments, three distinct concentration levels at low (10^{-10} M), medium (10^{-6} M), and high (10^{-3} M) concentrations were prepared, and the SERS spectra were obtained (Fig. S6†). Based on the Raman signal intensity at the marker peak of each sample, we obtained the measured concentrations according to the calibration curves shown in Fig. 7. The recovery rate of known amounts of spiked herbicides in tap water was calculated with respect to the spiked concentration and is reported in Table 1. The results indicate that the recovery rate at medium and high levels is >90%, higher than the lower level in the range of 87–88%. These results demonstrate the effectiveness of using AuNPs@CNDs for the detection of herbicides in tap water.

Table 1 Recovery rate (% = measured conc/spiked con. × 100) of spiked herbicides in tap water

Herbicide	Spiked herbicide (M)	Measured (M, averaged)	Recovery rate (%)
CGA77102	10^{-3}	0.95×10^{-3}	95 ± 2
	10^{-6}	9.66×10^{-7}	96 ± 1.8
	10^{-10}	6.73×10^{-11}	87 ± 1.5
A19414A	10^{-3}	0.95×10^{-3}	95 ± 2.1
	10^{-6}	9.82×10^{-7}	98 ± 1.2
	10^{-10}	8.71×10^{-11}	87 ± 1.9
ZA1296E	10^{-3}	0.87×10^{-3}	87 ± 4.8
	10^{-6}	9.91×10^{-7}	89 ± 3.0
	10^{-10}	7.69×10^{-11}	87 ± 4.0
A12738A	10^{-3}	0.88×10^{-3}	88 ± 1.0
	10^{-6}	9.61×10^{-7}	96 ± 1.1
	10^{-10}	8.71×10^{-11}	87 ± 3.5

3.5 A comparison of NP-based SERS detection of herbicides

To the best of our knowledge, SERS detection of herbicides mesotrione and S-metolachlor has been rarely reported in the literature. AuNPs or AgNP-based SERS substrates were used for the detection of a few other herbicides. Table 2 summarizes the representative work on herbicide detection, including the SERS substrates used, synthesis methods, detection ranges and sensitivities (LOD), for comparison with this work. This work, to the best of our knowledge, for the first time uses hybrid AuNPs@CNDs as SERS substrates for the detection of two herbicides and demonstrates superior sensitivity and a broad dynamic range of concentrations.

4. Conclusion

A hybrid AuNPs@CND SERS substrate was synthesized through a simple approach using CNDs as reducing and stabilizing agents. SERS substrates with different nominal mass ratios of CNDs to $HAuCl_4$ were evaluated using Rh6G and it turned out that a ratio of 2.4 provides the highest Raman enhancement response. The enhancement is believed to arise from electronic coupling at the interface of gold and carbon structures with a specific size and composition for an optimized localized electromagnetic field in SERS. The hybrid AuNPs@CND substrates produce a significant enhanced Raman signal with excellent response and almost an order of magnitude signal amplification in Rh6G measurements when compared to AuNPs or CNDs alone used as the SERS substrate. The SERS measurements of four different herbicide samples containing an active component, mesotrione or S-metolachlor, respectively, coupled to the hybrid substrate illustrate excellent repeatability, and reproducibility. Additionally, the long

Table 2 A summary of NP-based SERS detection of herbicides

Herbicides	SERS substrate	Synthesis method	Detection range	LOD (sensitivity)	Ref.
Paraquat	AgNPs@Si	*In situ* growth	1–1000 ppm	1 ppm	43
Atrazine	CNDs@AgNPs	Hydrothermal	10–1000 nM	10 nM (2 ppm)	44
Atrazine	Au nanorod array	Seed growth	0.01–10 mM	0.1 mM	26
Paraquat	AuNPs-3D structure	Laser engraving	2.7 ppb–27 ppm	2.7 ppb	45
Flumetsulam	AuNPs-$MgSO_4$	$HAuCl_4$ reduction	0.005–1 ppm	10 ppb	46
Glyphosate	Si-AgNPs		0.1–10 000 nM	0.01 nM	47
Diquat	Au nanobipyramids (AuBPs) MoS_2@tinfoil box	Layer-by-layer	1 pM–0.1 mM	1 pM (in urine)	48
Paraquat	Au nanostars	Seed growth	0.2–50 ppm	0.2 ppm	49
Prometryn	AgNPs	Colloidal synthesis	4.0–800 μM 8.0–800 μM	28 ppb (pH 11) 128 ppb (pH 7)	50
Atrazine	AgNPs@electrode	Colloidal synthesis	1 nm–1 mM	—	51
Paraquat	AuNPs-aptamer	Deposition on chip	0.25–2.5 μM	0.1 μM	52
Mesotrione	AuNPs@CNDs	Microwave-assisted	0.1 nM–1 mM	0.1 nM	This work
S-metolachlor			0.1 nM–1 mM	0.1 nM	

term stability demonstrated in this study for sensitive determination of the herbicides spiked in tap water promises for use in remote environmental areas.

Author contributions

Conceptualization, Jianjun Wei; data curation, Naghmeh Aboualigaledari, Panesun Tukur, Mengxin Liu and Frank Tukur; funding acquisition, Simona Murph and Jianjun Wei; investigation, Naghmeh Aboualigaledari, Anitha Jayapalan, Panesun Tukur, Mengxin Liu and Frank Tukur; methodology, Naghmeh Aboualigaledari, Anitha Jayapalan, Yanling Zhang and Jianjun Wei; project administration, Jianjun Wei; resources, Gerald Ducatte, Madan Verma, Janet Tarus and Simona Murph; supervision, Simona Murph and Jianjun Wei; writing – original draft, Naghmeh Aboualigaledari; and writing – review & editing, Jianjun Wei.

Data availability

The datasets supporting this article have been uploaded as part of the ESI.†

Conflicts of interest

The authors declare no competing financial interest.

Acknowledgements

This work was supported by the Department of Energy Minority Serving Institution Partnership Program (MSIPP) managed by the Savannah River National Laboratory under BSRA contract TOA # 0961 (G-SOW-A-02375) and by a Syngenta Inc. (Greensboro, NC, USA) grant *via* a Cooperative Agreement (PO# 1400105841).

This work was performed at the JSNN, a member of the Southeastern Nanotechnology Infrastructure Corridor (SENIC) and the National Nanotechnology Coordinated Infrastructure (NNCI), which is supported by the National Science Foundation (ECCS-1542174).

References

1 V. M. Pathak, V. K. Verma, B. S. Rawat, B. Kaur, N. Babu, A. Sharma, S. Dewali, M. Yadav, R. Kumari, S. Singh, A. Mohapatra, V. Pandey, N. Rana and J. M. Cunill, *Front. Microbiol.*, 2022, **13**, 962619.
2 J. Kvalvåg, *Analyst*, 1974, **99**, 666–669.
3 E.-C. Zhao, W.-L. Shan, S.-R. Jiang, Y. Liu and Z.-Q. Zhou, *Microchem. J.*, 2006, **83**, 105–110.
4 Y. Wang, L. Shen, Z. Gong, J. Pan, X. Zheng and J. Xue, *Water Environ. Res.*, 2019, **91**, 1009–1024.
5 W. L. Budde, *Mass Spectrom. Rev.*, 2004, **23**, 1–24.
6 S. G. Han and T. G. Nam, *Appl. Biol. Chem.*, 2024, **67**, 12.
7 H. Du, Y. Xie and J. Wang, *TrAC, Trends Anal. Chem.*, 2021, **135**, 116178.
8 R. D. Ayivi, S. O. Obare and J. Wei, *TrAC, Trends Anal. Chem.*, 2023, **167**, 117231.
9 R. D. Ayivi, B. O. Adesanmi, E. S. McLamore, J. Wei and S. O. Obare, *Chemosensors*, 2023, **11**, 203.
10 A. I. Pérez-Jiménez, D. Lyu, Z. Lu, G. Liu and B. Ren, *Chem. Sci.*, 2020, **11**, 4563–4577.
11 Á. I. López-Lorente, *Anal. Chim. Acta*, 2021, **1168**, 338474.
12 Z. Zeng, Y. Liu and J. Wei, *TrAC, Trends Anal. Chem.*, 2016, **75**, 162–173.
13 S. H. Murph, G. K. Larsen and K. J. Coopersmith, *Anisotropic and Shape-Selective Nanomaterials: Structure-Property Relationships*, Springer Cham, 1st edn, 2017.
14 Shinki and S. Sarkar, in *Encyclopedia of Materials: Electronics*, ed. A. S. M. A. Haseeb, Academic Press, Oxford, 2023, pp. 442–458, DOI: **10.1016/B978-0-12-819728-8.00051-6**.
15 W. Wu and M. Pauly, *Mater. Adv.*, 2022, **3**, 186–215.
16 Y. Guo, Z. Xu, A. G. Curto, Y.-J. Zeng and D. Van Thourhout, *Prog. Mater. Sci.*, 2023, **138**, 101158.
17 H. Yu, W. Wu and Z.-Y. Li, in *Encyclopedia of Nanomaterials*, ed. Y. Yin, Y. Lu and Y. Xia, Elsevier, Oxford, 1st edn, 2023, pp. 496–510, DOI: **10.1016/B978-0-12-822425-0.00045-2**.
18 K. Bhardwaj and A. Jaiswal, *Analyst*, 2023, **148**, 562–572.
19 N. V. Doroshina, O. A. Streletskiy, I. A. Zavidovskiy, M. K. Tatmyshevskiy, G. I. Tselikov, O. O. Kapitanova, A. V. Syuy, R. Romanov, P. Mishra, V. Bobrovs, A. M. Markeev, D. I. Yakubovsky, I. A. Veselova, A. V. Arsenin, V. S. Volkov and S. M. Novikov, *Heliyon*, 2024, **10**, e27538.
20 K. Sridhar, B. S. Inbaraj and B.-H. Chen, *Chemosphere*, 2022, **301**, 134702.
21 F. D. Cortes Vega, P. G. Martinez Torres, J. Pichardo-Molina, N. M. Gomez Ortiz, V. G. Hadjiev, J. Zarate Medina and F. C. Robles Hernandez, *J. Mater. Chem. C*, 2017, **5**, 4959–4966.
22 J. Son, G.-H. Kim, Y. Lee, C. Lee, S. Cha and J.-M. Nam, *J. Am. Chem. Soc.*, 2022, **144**, 22337–22351.
23 H. Chen, Z. Cheng, X. Zhou, R. Wang and F. Yu, *Anal. Chem.*, 2022, **94**, 143–164.
24 D. García-Lojo, S. Núñez-Sánchez, S. Gómez-Graña, M. Grzelczak, I. Pastoriza-Santos, J. Pérez-Juste and L. M. Liz-Marzán, *Acc. Chem. Res.*, 2019, **52**, 1855–1864.
25 J. Langer, D. Jimenez de Aberasturi, *et al.*, *ACS Nano*, 2020, **14**, 28–117.
26 N. Albarghouthi, P. MacMillan and C. L. Brosseau, *Analyst*, 2021, **146**, 2037–2047.
27 J.-F. Li, Y.-J. Zhang, S.-Y. Ding, R. Panneerselvam and Z.-Q. Tian, *Chem. Rev.*, 2017, **117**, 5002–5069.
28 G. K. Larsen, W. Farr and S. E. H. Murph, *J. Phys. Chem. C*, 2016, **120**, 15162–15172.

29 E. G. d. L. Oliveira, H. P. de Oliveira and A. S. L. Gomes, *SN Appl. Sci.*, 2020, **2**, 1491.
30 T. Wang, S. Wang, Z. Cheng, J. Wei, L. Yang, Z. Zhong, H. Hu, Y. Wang, B. Zhou and P. Li, *Chem. Eng. J.*, 2021, **424**, 130323.
31 J. Liu, R. Li and B. Yang, *ACS Cent. Sci.*, 2020, **6**, 2179–2195.
32 D. M. Arvapalli, A. T. Sheardy, K. C. Alapati and J. Wei, *Talanta*, 2020, **209**, 120538.
33 Z. Ji, A. Sheardy, Z. Zeng, W. Zhang, H. Chevva, K. Allado, Z. Yin and J. Wei, *Molecules*, 2019, **24**, 152.
34 Z. Ji, Z. Yin, Z. Jia and J. Wei, *Langmuir*, 2020, **36**, 8632–8640.
35 H. Safardoust-Hojaghan, O. Amiri, M. Hassanpour, M. Panahi-Kalamuei, H. Moayedi and M. Salavati-Niasari, *Food Chem.*, 2019, **295**, 530–536.
36 S. Khan and A. K. Narula, *J. Mater. Sci.*, 2023, **34**, 1955.
37 N. Far'ain Md Noor, M. A. Saiful Badri, M. M. Salleh and A. A. Umar, *Opt. Mater.*, 2018, **83**, 306–314.
38 M. Azami, J. Wei, M. Valizadehderakhshan, A. Jayapalan, O. O. Ayodele and K. Nowlin, *J. Phys. Chem. C*, 2023, **127**, 7360–7370.
39 R. Das, S. Parveen, A. Bora and P. K. Giri, *Carbon*, 2020, **160**, 273–286.
40 L. Wang, C. Li, Y. Luo and Z. Jiang, *Materials*, 2018, **11**, 1655.
41 Z. Zeng, W. Zhang, D. M. Arvapalli, B. Bloom, A. Sheardy, T. Mabe, Y. Liu, Z. Ji, H. Chevva, D. H. Waldeck and J. Wei, *Phys. Chem. Chem. Phys.*, 2017, **19**, 20101–20109.
42 M. Berge, A. Dowek, P. Prognon, F.-X. Legrand, A. Tfayli, L. Minh Mai Lê and E. Caudron, *Spectrochim. Acta, Part A*, 2022, **268**, 120628.
43 T. C. Dao, T. Q. N. Luong, T. A. Cao, N. H. Nguyen, N. M. Kieu, T. T. Luong and V. V. Le, *Adv. Nat. Sci.: Nanosci. Nanotechnol.*, 2015, **6**, 035012.
44 J. Tang, W. Chen and H. Ju, *Talanta*, 2019, **201**, 46–51.
45 R. Botta, P. Eiamchai, M. Horprathum, S. Limwichean, C. Chananonnawathorn, V. Patthanasettakul, R. Maezono, A. Jomphoak and N. Nuntawong, *Sens. Actuators, B*, 2020, **304**, 127327.
46 M. Han, H. Lu and Z. Zhang, *Molecules*, 2020, **25**, 4662.
47 K. A. López-Castaños, L. A. Ortiz-Frade, E. Méndez, E. Quiroga-González, M. A. González-Fuentes and A. Méndez-Albores, *Front. Chem.*, 2020, **8**, 612076.
48 Q.-Y. Jiang, D. Li, Y. Liu, Z.-S. Mao, Y. Yu, P. Zhu, Q. Xu, Y. Sun, L. Hu, J. Wang, J. Chen, F. Chen and Y. Cao, *Sens. Actuators, B*, 2021, **344**, 130290.
49 M.-H. Lin, L. Sun, F. Kong and M. Lin, *Food Control*, 2021, **130**, 108280.
50 R. J. G. Rubira, L. N. Furini, C. J. L. Constantino and S. Sanchez-Cortes, *Vib. Spectrosc.*, 2021, **114**, 103245.
51 N. Albarghouthi, M. M. Eisnor, C. C. Pye and C. L. Brosseau, *J. Phys. Chem. C*, 2022, **126**, 9836–9842.
52 N. Kamkrua, T. Ngernsutivorakul, S. Limwichean, P. Eiamchai, C. Chananonnawathorn, V. Pattanasetthakul, R. Ricco, K. Choowongkomon, M. Horprathum, N. Nuntawong, T. Bora and R. Botta, *ACS Appl. Nano Mater.*, 2023, **6**, 1072–1082.
53 P. Luo, C. Li and G. Shi, *Phys. Chem. Chem. Phys.*, 2012, **14**, 7360–7366.
54 G. Frens, *Nat. Phys. Sci.*, 1973, **241**, 20–22.
55 X. Miao, S. Wen, Y. Su, J. Fu, X. Luo, P. Wu, C. Cai, R. Jelinek, L.-P. Jiang and J.-J. Zhu, *Anal. Chem.*, 2019, **91**, 7295–7303.
56 H. Al-Johani, E. Abou-Hamad, A. Jedidi, C. M. Widdifield, J. Viger-Gravel, S. S. Sangaru, D. Gajan, D. H. Anjum, S. Ould-Chikh, M. N. Hedhili, A. Gurinov, M. J. Kelly, M. El Eter, L. Cavallo, L. Emsley and J.-M. Basset, *Nat. Chem.*, 2017, **9**, 890–895.
57 Y. Lyu, L. M. Becerril, M. Vanzan, S. Corni, M. Cattelan, G. Granozzi, M. Frasconi, P. Rajak, P. Banerjee, R. Ciancio, F. Mancin and P. Scrimin, *Adv. Mater.*, 2024, **36**, 2211624.
58 B. Bagra, W. Zhang, Z. Zeng, T. Mabe and J. Wei, *Langmuir*, 2019, **35**, 8903–8909.
59 B. D. Mansuriya and Z. Altintas, *Nanomaterials*, 2021, **11**, 2525.
60 N. Naskar, M. Wagner, H. J. Räder, H. Qi, U. Kaiser, T. Weil and S. Chakrabortty, *Adv. Photonics Res.*, 2022, **3**, 2100092.
61 R. Liu, H. Huang, H. Li, Y. Liu, J. Zhong, Y. Li, S. Zhang and Z. Kang, *ACS Catal.*, 2014, **4**, 328–336.
62 X. Fei, Z. Liu, Y. Li, G. Yang, C. Su, H. Zhong, Z. Zhuang and Z. Guo, *J. Alloys Compd.*, 2017, **725**, 1084–1090.
63 H. Qiu, M. Wang, M. Cao, L. Zhang, S. Ji, J. Dou, Y. Ji, S. Kou, J. Guo and Z. Yang, *Appl. Surf. Sci.*, 2019, **489**, 1010–1018.
64 M. Ayiania, M. Smith, A. J. R. Hensley, L. Scudiero, J.-S. McEwen and M. Garcia-Perez, *Carbon*, 2020, **162**, 528–544.
65 Z. Zeng, T. Mabe, W. Zhang, B. Bagra, Z. Ji, Z. Yin, K. Allado and J. Wei, *ACS Appl. Bio Mater.*, 2018, **1**, 802–807.
66 J. Waitkus, Y. Chang, L. Liu, S. V. Puttaswamy, T. Chung, A. M. Molina Vargas, S. J. Dollery, M. R. O'Connell, H. Cai, G. J. Tobin, N. Bhalla and K. Du, *Adv. Mater. Interfaces*, 2023, **10**, 2201261.
67 X. N. He, Y. Gao, M. Mahjouri-Samani, P. N. Black, J. Allen, M. Mitchell, W. Xiong, Y. S. Zhou, L. Jiang and Y. F. Lu, *Nanotechnology*, 2012, **23**, 205702.
68 C. Kavitha, K. Bramhaiah, N. S. John and B. E. Ramachandran, *Chem. Phys. Lett.*, 2015, **629**, 81–86.
69 P. Vítek, K. Novotná, P. Hodaňová, B. Rapantová and K. Klem, *Spectrochim. Acta, Part A*, 2017, **170**, 234–241.